Computer-Aided Civil and Infrastructure Engineering **28** (2013) 289–306

Prioritization of Code Development Efforts in Partitioned Analysis

Joshua Hegenderfer & Sez Atamturktur*

Glenn Department of Civil Engineering, Clemson University, Clemson, SC, USA

Abstract: *In partitioned analysis of systems that are driven by the interaction of functionally distinct but strongly coupled constituents, the predictive accuracy of the simulation hinges on the accuracy of individual constituent models. Potential improvement in the predictive accuracy of the simulation that can be gained through improving a constituent model depends not only on the relative importance, but also on the inherent uncertainty and inaccuracy of that particular constituent. A need exists for prioritization of code development efforts to cost-effectively allocate available resources to the constituents that require improvement the most. This article proposes a novel and quantitative code prioritization index to accomplish such a task and demonstrates its application on a case study of a steel frame with semirigid connections. Findings show that as high-fidelity constituent models are integrated, the predictive ability of model-based simulation is improved; however, the rate of improvement is dependent upon the sequence in which the constituents are improved.*

1 INTRODUCTION

Numerical simulation has become a viable tool for investigating complex physical systems and processes that are encountered in many civil engineering disciplines, especially when solely experiment-based, empirical studies are infeasible. Although numerical models offer versatility in simulating various operational conditions or design scenarios, they can only provide an approximation of reality, and thus, there is a need to check the validity of model solutions against experimental observations. Numerical models therefore, come with the burden of quantifying the uncertainties and biases in model predictions through tasks that fall under the broad concept of *model validation*.

*To whom correspondence should be addressed. E-mail: *sez@clemson.edu.*

To guide the model validation efforts, many frameworks, such as those presented in Unal et al. (2011), Jung (2011), Bayarri et al. (2007), and Jiang and Mahadevan (2007), have been developed to rigorously and quantitatively assess model biases and uncertainties (Figure 1). Each of these frameworks demonstrates that model validation efforts can be improved through either additional experimentation or further code development. If additional experimentation is necessary, the efficient and optimal selection of experimental settings can be achieved through algorithms such as those presented in Jiang and Mahadevan (2007) and Williams et al. (2011). However, if code development is selected as the next step in model validation, the particular elemental components of the numerical model requiring more sophisticated modeling of physics or engineering principles remains unknown. Naturally, unlimited time and resources would render the prioritization of such code development efforts irrelevant. However, given the inevitable limitations in resources, major model deficiencies must be pinpointed and code development efforts must be focused to achieve the greatest reduction in model uncertainty and bias. The scientific problem of code prioritization has been studied to optimize software fault detection (Korel, 2009) and parallel processing of finite element (FE) computer codes (Zeyao and Lianxiang, 2004); however, quantitative approaches for code prioritization of complex numerical models are lacking in the published literature.

Such need becomes especially amplified for complex, heterogonous systems that are driven by the interaction of functionally distinct but strongly coupled constituents commonly tackled by partitioned analysis procedures. Our focus is therefore on models that comprise multiple, isolated, components (or substructures), herein referred to as *constituents*. These constituents interact to form a collective system, herein referred to as *coupled model*. Such focus is relevant as many numerical models in civil and infrastructure

DOI: 10.1111/j.1467-8667.2012.00799.x

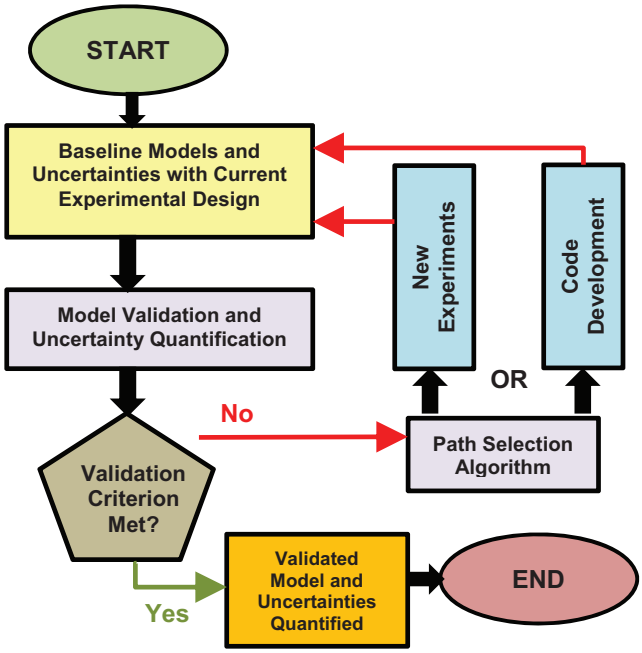

Fig. 1. Generic model validation framework.

engineering are indeed coupled models that are an amalgam of multiple constituents or systems of constituents; see, for instance, the published literature on soil–structure interaction (Provenzano, 2003; Qian and Zhang, 1993), fluid–structure interaction (Kutay and Aydilek, 2009; Caracoglia et al., 2009), human–structure interaction (Macdonald, 2009; Wang et al., 2011), and the broad field of substructuring (or subdomains), which essentially focuses on structure–structure interaction (Mahjoubi et al., 2009; Mahjoubi et al., 2011). While aiming to improve the predictive accuracy of such coupled simulation models, one obvious question arises: to achieve the greatest reduction in model uncertainty and bias, which constituent must be given the highest priority for further code development?

This article presents a code prioritization approach for coupled numerical models through the use and extension of a well-established ranking system, in which code development efforts are guided to effectively improve the predictive capability of the coupled model. A novel, quantitative code prioritization index (CPI) is proposed and demonstrated using a proof-of-concept example, in which the structural system consists of a two-story steel frame built in the laboratory with semirigid connections. An initial, simplified FE model is developed for the frame system using beam elements, where the beam-to-column connections can be modeled as either fixed or pinned connections, neither of which are representative of reality. One approach commonly utilized in the literature entails adding fictitious *knobs* (empirical or arbitrary parameters used in place of detailed physics modeling) to represent these inherently semirigid connections. This initial FE model can then be improved by refining the definition of these knobs, such as through the development of high-fidelity three-dimensional, nonlinear FE models (constituents). Three possible constituent connection models are identified to be coupled to the initial simplified frame FE model. These three constituents are ranked using the proposed CPI that combines knowledge level, importance, and error contribution. The frame model is then improved incrementally by coupling the three high-fidelity connection models in the sequence selected by CPI, and the resulting improvement in predictive accuracy of the coupled model is quantified.

The article is organized as follows: Section 2 overviews the pertinent literature on coupling algorithms and ranking procedures that are used as the foundation for the CPI described in Section 3. Section 4 introduces the case study application, in which the predictions of the initially inexact FE model of the steel frame are compared against experimentally obtained static and dynamic characteristics. In Section 5, the CPI is deployed to rank model constituents, which are developed, verified, and validated in Section 6. The coupling procedure used to integrate the constituent models to the frame model is described in Section 7. Section 8 presents a comparison of the initial FE model as well as its improved variants against experimental data. Finally in Section 9, concluding remarks are made, limitations of the proposed approach are summarized, and the future direction is overviewed.

2 BACKGROUND

2.1 Phenomenon identification and ranking table

Originally proposed as part of the U.S. Nuclear Reactor Commission's (NRC) Code Scaling, Applicability, and Uncertainty (CSAU) evaluation procedure (Boyack et al., 1989), the Phenomenon Identification and Ranking Table (PIRT) is currently being used by the U.S. NRC at the start of new programs to rank constituent phenomena from the perspective of resource allocation (ARRIA, 2003; Olivier and Nowlen, 2008; Tregoning et al., 2009). The purpose of PIRT is to effectively gather expert opinion about the importance and knowledge level of a set of phenomena (Diamond, 2006). The PIRT process, typically completed by a committee of multidisciplinary experts, provides a systematic, structured, and hierarchical methodology to rank phenomena of interest for resource allocation problems (Boyack, 2009). The two major scoring components of PIRT, (1) the importance of a phenomena and

(2) the level of current knowledge, constitute the particular phenomena's sensitivity or impact on the evaluation metric and the current lack of knowledge about the phenomena (and/or parameters associated with that phenomena), respectively. Although historically PIRT has mainly been used in the nuclear reactor and safety fields, the general and high-level approach of the PIRT process makes it highly adaptable to many different areas of science and engineering.

2.2 Partitioned analysis procedures

In partitioned analysis procedures, constituent models are viewed as discrete entities with data transferred at the interface between the individual constituent codes through coupling algorithms (Rugonyi and Bathe, 2001; Xiong et al., 2011). This type of analysis most often results in an iterative procedure involving prediction, substitution, and organization techniques (Felippa et al., 2001; Larson et al., 2005; Larson, 2009). The advantage of the partitioned approach stems from the ability to exploit independent modeling strategies developed in different domains (Leiva et al., 2010) in addition to time and space discretization that is most appropriate for each constituent (Kassiotis et al., 2011; Joosten et al., 2009). This flexibility obtains solutions for highly complex coupled problems while making efficient use of well-established codes and expert knowledge in various fields (Ibrahimbegović et al., 2004). Furthermore, the ability to solve complex problems through integrated parallelization on multiple sets of processors can make the partitioned approach particularly efficient (Park and Felippa, 1983; Adeli and Kamal, 1993).

Coupling is most commonly classified according to the nature of the mutually dependent parameters. In weak coupling (also known as loose or explicit coupling), the state of the constituents does not mutually interact with each other's inputs or outputs (Matthies and Steindorf, 2002a; Wang et al., 2004). In partitioned analysis, if the state of the constituents is affected by model outputs, the coupling interface is referred to as strong coupling (also known as tight or implicit coupling) (Matthies and Steindorf, 2003; Zhang and Hisada, 2004). In strong coupling, the repeated execution of constituent models to achieve self-consistent state solutions becomes necessary (Ramanath, 2011). Input parameters in strong coupling problems are defined as either dependent or independent. The dependent input parameters are functions of the output of another constituent; therefore, the coupling algorithm must evaluate and substitute these parameters as input for the appropriate constituent. Finding the correct values for these dependent variables is the main question to be solved in strong coupling problems. Various

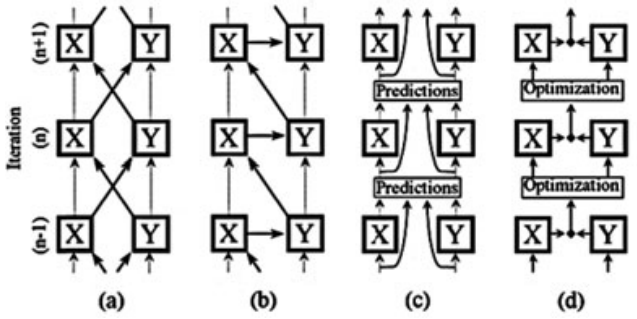

Fig. 2. Coupling algorithms: (a) Block-Jacobi, (b) Block Gauss-Seidel, (c) Block Newton, and (d) optimization-based coupling.

strong coupling algorithms are proposed in the literature (Figures 2a–d): the Block-Jacobi method (Matthies et al., 2006; Fernandez and Moubachir, 2005), the Block Gauss-Siedel method (Joosten et al., 2009; Matthies et al., 2006), gradient-based Newton-like methods (Heil, 2004; Matthies and Steindorf, 2002b; Matthies and Steindorf, 2003; Fernandez and Moubachir, 2005), and optimization-based methods (Farajpour and Atamturktur, 2012).

Note that in partitioned analysis, quantification, propagation, and mitigation of uncertainties in input parameters play an important role for the complete validation of coupled models (Avramova and Ivanov, 2010), which is currently an active research area. The focus of this article, however, is exclusively on improved sophistication of constituent models to reduce the systematic bias in coupled models predictions; therefore, uncertain input parameters are treated as deterministic best estimates.

3 CODE PRIORITIZATION INDEX

The PIRT, overviewed in Section 2.1, supplies an inherently qualitative and subjective evaluation of a system that is driven by the interaction of coupled constituent phenomena. As such, this section details the transformation of PIRT into a quantitative approach through the CPI. Following an approach similar to Hemez et al. (2010), CPI is formulated considering the three factors that determine the importance a constituent has on the overall predictive accuracy of a coupled simulation: (1) the sensitivity of the coupled system behavior to the constituent output, (2) the estimated biases in the constituent output, and (3) the estimated uncertainties in the constituent. CPI, therefore, takes the following form:

$$CPI_i = \|SA_i\| \times \|EA_i\| \times \|UA_i\| \qquad (1)$$

where SA_i, EA_i, and UA_i, respectively, represent the importance (*Sensitivity Analysis*), estimated error

(*Error Analysis*), and current level of knowledge (*Uncertainty Analysis*) for a given constituent *i*, in an appropriately chosen norm, $\| \bullet \|$.

3.1 Sensitivity analysis (SA)

The SA term is defined as the measure of the variability in the model output due to unit variability in a given constituent. This term can be quantified using various established screening, local or global sensitivity analysis techniques; however, for complex problems that are nonlinear in nature and that involve a large number of input parameters of varying uncertainty, global sensitivity analysis techniques should be preferred (Cukier et al., 1978). The global sensitivity analysis inherently takes the range and shape of the probability distributions of input parameters into account. Moreover, in global sensitivity analysis techniques, such as the analysis of variance (ANOVA) (Moaveni et al., 2009; Frey and Patil, 2002), the sensitivity estimates for each parameter are computed in the presence of uncertainty of all other factors of interest; thus taking the possible correlations and dependencies between input parameters into consideration.

3.2 Error analysis (EA)

The EA term is a representative estimate of a constituent's error contribution to the total error of the system in comparison to the experimental evidence. This term can be quantified using various metrics including model form error estimates for separate effect experiments as defined in Higdon et al. (2008), Oberkampf and Barone (2006), Rebba et al. (2006), and Atamturktur et al. (2011).

In this study, for a given constituent, EA is defined as a measure of the constituent "correction" necessary such that error in the coupled model predictions is minimized (given a set of uncertainty attributed to other constituents) as shown in Equations (2) and (3)

$$P_j = \{P : \delta_j(P, \alpha) < \delta_j^t\} \tag{2}$$

$$EA = \frac{1}{n}\sum_{j=1}^{n} \left(\min \left| P_0 - P_j \right|\right) / P_0 \tag{3}$$

where n is the number of experiments; P_0 represents the nominal value for the fictitious knob; P_j is the selected parameter value for the constituent at the jth experiment; $\delta_j(P, \alpha)$ is the discrepancy of the constituent at the jth experiment defined as a function of collective parameters of the constituents; and α is the uncertainty assigned to all other uncertain parameters. The δ_j^t is the discrepancy threshold value at the jth experiment for the constituent of interest, which is derived in Equations (4)–(7).

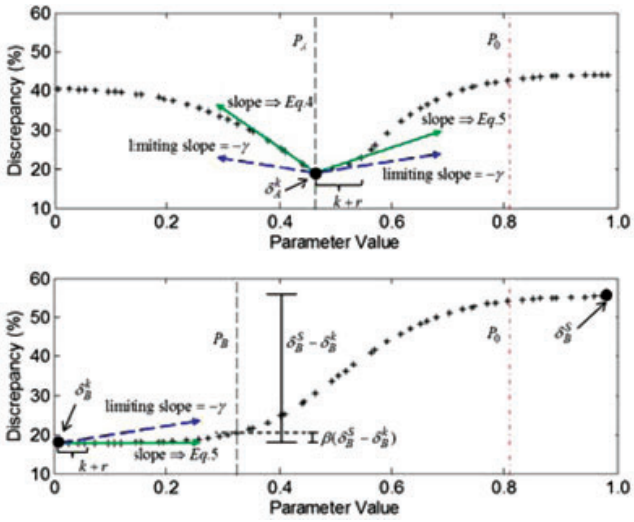

Fig. 3. Computation of P_j: absolute minimum discrepancy: Equation (6) (top) and converged minimum discrepancy: Equation (7) (bottom).

An absolute minimum discrepancy exists if Equations (4) and (5) given below are both satisfied.

$$\frac{\delta_j^k - \delta_j^{k-r}}{P(\delta_j^k) - P(\delta_j^{k-r})} < -\gamma \tag{4}$$

$$\frac{\delta_j^{k+r} - \delta_j^k}{P(\delta_j^{k+r}) - P(\delta_j^k)} < +\gamma \tag{5}$$

where γ is the limiting slope as indicated in Figure 3 and r represents the number of runs over which the slope is computed (see Figure 3); k is the index number of computer runs corresponding to the minimum discrepancy over all simulation runs; and δ_j^k is the minimum computed discrepancy across all simulation runs. In this case, the threshold value for discrepancy is selected according to Equation (6); otherwise, a converged minimum discrepancy exists and the threshold value for discrepancy is calculated according to Equation (7);

$$\delta_j^t = \delta_j^k \tag{6}$$

$$\delta_j^t = \beta\left(\delta_j^S - \delta_j^k\right) + \delta_j^k \tag{7}$$

where β represents a percentage of the total allowable reduction discrepancy to limit excessive changes in the nominal value of the knob (see Figure 3) and δ_j^S represents the maximum computed discrepancy across all simulation runs.

The EA term in Equation (3) seeks to determine the necessary deviation from the initial parameter value over all available experiments such that the relative

difference between model predictions and experimental results (referred to herein as discrepancy) is minimized. To achieve this minimization, the numerical model parameters of interest are sampled within a plausible range defined for parameter of interest, P, and a set percentage variability, α, for all other parameters, thus accounting for potential cross-correlations between parameters through the α variability term. Computer runs can be generated using various sampling designs that thoroughly explore possible values for P in an efficient manner. The EA value realized from Equation (3) is represented as a percentage of the initially assumed parameter value, P_0. Therefore, higher EA values indicate a greater estimated error for the parameter of interest.

The values of r, γ, and β (from Equations (4)–(7)) are assigned according to the specific application of interest. If discrepancy throughout the investigated domain is constant (the calculated slope is below the limiting value of γ) or if the discrepancy behavior is divergent for any specific experiment j, then a meaningful and confident evaluation of P_j is difficult. Thus, if the given experiment is not sensitive to parameter P, a selection of P_j would be unfounded; therefore, the contribution from such experiments is excluded from the analysis.

Note that if model calibration of constituents is completed prior to the utilization of the CPI metric, the calibrated parameter values for the parameters would be used as the initial values for the EA analysis. When such calibration activities are not available *a priori*, the proposed method gives the best possible guidance by directing the focus of the decision makers and code developers to the constituent that is mostly responsible for the inaccuracies of the coupled model prediction. The inaccuracies in the selected constituent may originate from either the incompleteness of the modeled physics or engineering principles or the imprecision in the model parameters.

3.3 Uncertainty analysis (UA)

The UA term can be quantified for a particular model constituent according to experimental test results or qualitative expert opinion. Herein, however, the current level of knowledge, that is, uncertainty analysis, for each constituent will be treated as a binary number, where zero represents a phenomenon for which the knowledge level is mature and where one represents a phenomenon that is not yet well known. In effect, as recommended in the PIRT construction process, the UA term restricts code prioritization efforts only to poorly or partially understood phenomena.

Therefore, the CPI term is maximized when SA, EA, and UA are all high. Herein, a type of norm for each of the CPI terms is chosen such that each term is scaled to a maximum of one over all possible constituents; therefore, CPI values are, without loss of generality, bounded between zero and one, and higher CPI terms are considered as higher priority.

Fig. 4. Frame structure built in the laboratory (left) and frame connections (right): top connection (top), middle connection (middle), base connection (bottom).

4 OVERVIEW OF THE CASE STUDY APPLICATION

4.1 Case study structure: laboratory specimen

The small-scale, prototype structure is a two-story single-bay steel frame shown in Figure 4, in which all members of the frame are made of A36 mild steel. The connections are secured with two SAE J429—Grade 5 bolts on each side, and all bolts are torqued to 9.0 Nm. The geometric dimensions of the test frame are given in Table 1.

4.2 Initial numerical model

The baseline FE model for the frame (henceforth referred to as Model #1) is created in ANSYS v.13.0 using BEAM188 elements as shown in Figure 5. These are two-noded six-degrees-of-freedom per node linear elements that consider the cross-section and orientation of the member (ANSYS, 2010). An isotropic linear elastic constitutive model is used with Young's modulus specified as 200 GPa (29,000 ksi) and Poisson's ratio as 0.33, which are typical values for mild structural steel.

Table 1
Geometric properties of the laboratory frame structure

Steel frame member geometric properties			
Member	*Length (cm)*	*Cross-section type*	*Cross-section dimensions (cm)*
Columns	63.5	Angle	5.08 × 5.08 × 0.32
Beam	124.46	Flat	5.08 × 0.32
Base connecting tabs	5.08	Angle	5.08 × 5.08 × 0.32
Column base plates	1.27	Flat	15.24 × 15.24
Frame base	1.27	Flat	121.92 × 243.84
Bolt properties			
Bolt type		Bolt diameter (cm)	
SAE J429—Grade 5		0.66	

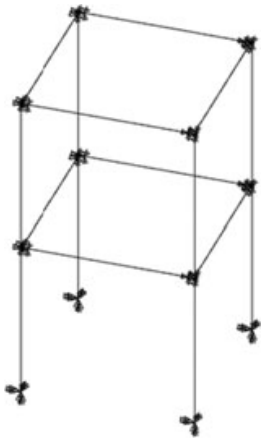

Fig. 5. Baseline FE model (Model #1) for the frame structure.

Similar to the approach used by Zapico et al. (2008), geometric offsets are considered when modeling the beam-to-column connections (also known as modeling to centroid). The two-bolt connections of the frame are expected to exhibit semirigid behavior with unknown stiffness characteristics.

In the literature, such semirigid connections are often approximated as either fixed or pinned depending upon the number of bolts, the bolt pattern, and expert judgment (Lee and Moon, 2002; Galvão et al., 2010). Therefore, an initial numerical model (Model #1) is built with similar approximations commonly implemented in practice. For Model #1, to determine a suitable connection type, either fixed or pinned connection, model predictions are compared against experimentally obtained static and dynamic response. In the fixed model, all connections are assumed to be fixed. However, for stability, in the pinned model the rotational degrees of freedom at the base connections as well as the top- and middle-level torsional degrees of freedom are fixed, while all remaining rotational degrees of freedom at the top and middle levels are pinned. After the selection of a suitable connection type, Model #1 will ultimately be used as a reference while determining the improvement gained in predictive accuracy by refining the way in which beam-to-column connections are represented in the FE model.

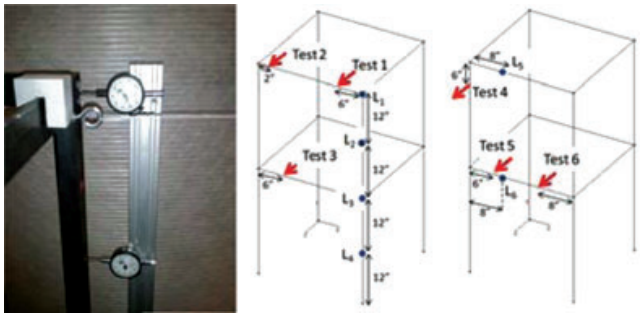

Fig. 6. Static experiment setup: cable and pulley system (left), measurement locations (right).

4.3 Experimental campaign

4.3.1 Static testing. Static testing is conducted using a cable and pulley system designed to apply a point load in the horizontal direction as shown in Figure 6. Federal C8IS Dial Deflection indicators are positioned at the locations shown in Figure 6 to measure horizontal deflection. Six separate static tests are conducted using point loads with increased amplitude and applied at a different location on the structure as shown in Figure 6, while displacements are measured at four points (L_1–L_4) along a single column for Tests 1–3 and two points (L_5 and L_6) on the beams for Tests 4–6. The displacement results for the static tests, shown in Figure 7, are compared to both the pinned and fixed connection FE models in Table 2. The static tests are completed at force levels where the material has not yielded, that is, it is still in the elastic regime as is demonstrated in the linear response shown in Figure 7.

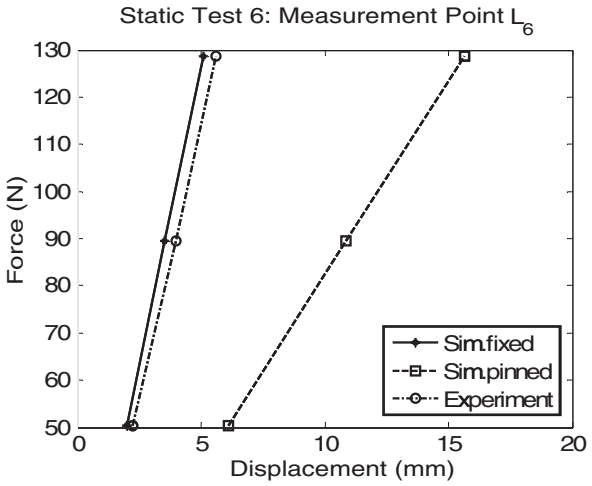

Fig. 7. Static test comparison between two alternative FE models (pinned connections and fixed connections) and experimental data.

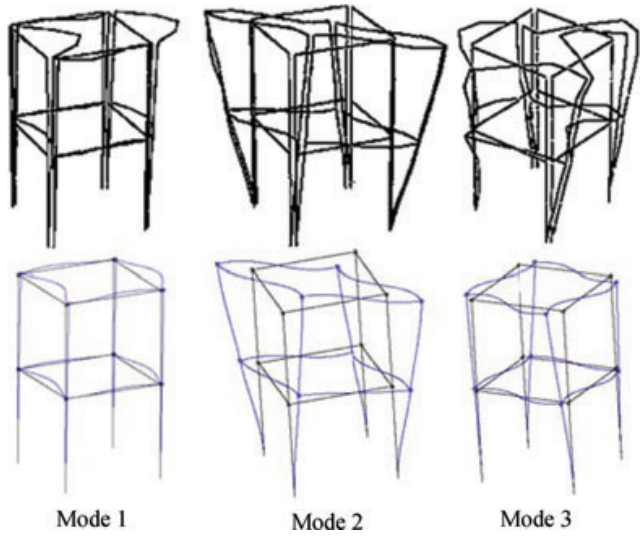

Fig. 8. Mode shapes: experimental testing (top) and FE model predictions (bottom).

4.3.2 Modal testing. Model 4507B Brüel and Kjær (B&K) unidirectional accelerometers are distributed to 88 locations, 6 inches apart throughout all beams and columns (see Figure 4), and a Model 8207 B&K modal impact hammer is used to excite the structure. Each hammer strike is repeated five times to reduce degrading effects of noise through averaging. Using Reflex software from B&K, natural frequencies (see Table 3) and mode shapes (see Figure 8) are extracted from the experimental data. The rational fraction polynomial parameter estimation technique (Richardson and Formenti, 1982) is implemented to generate stability diagrams for mode selection. The first three global modes of the structure are identified as shown in Figure 8 and listed in Table 3. As a means of verifying the orthogonality of the experimentally collected modes, the modal assurance criterion (MAC) (Allemang, 2003) is calculated (Table 4). The low off-diagonal terms in Table 4 demonstrate the linear independence of each of the experimentally determined modes.

Table 4
MAC of experimentally collected modes

Mode	*1*	*2*	*3*
1	1	0.003	0.002
2	0.003	1	0.001
3	0.002	0.001	1

4.4 Test-analysis correlation

Tables 2 and 3 show that the baseline model with fixed connections underestimates the deformations and overestimates the natural frequencies, while the baseline model with pinned connections overestimates the

Table 2
Comparison of baseline models and experimental data for static tests

Test	*1*	*2*	*3*	*4*	*5*	*6*	*Mean*
Fixed FE average error (%)	44.4	84.8	55.6	46.8	24.3	18.9	45.8
Pinned FE average error (%)	32.8	196.5	76.7	18.8	100.5	126.3	91.9

Table 3
Natural frequencies from experimental testing and baseline models

Mode	*Description*	*Test frequency (Hz)*	*Fixed FE frequency (Hz)*	*Error (%)*	*Pinned FE frequency (Hz)*	*Error (%)*
1	Sway	23.09	27.97	21.13	16.30	29.41
2	Bending	29.58	33.21	12.27	14.01	52.64
3	Torsion	37.04	47.56	28.40	25.96	29.91

deformations and underestimates the natural frequencies. As seen, neither the fixed nor the pinned connections are suitable to represent the connections of the frame of interest. However, the FE model with fixed connections more accurately predicts the static tests with a 46.1% lower average error than the FE model with pinned connections. Also, the FE model with fixed connections predicts the values of the natural frequencies in the correct order of modes, while pin connections yield an incorrect mode sequence.

Although the FE model with fixed connections yields a closer agreement to experiments and has been selected as the connection type to be used in Model #1, it still has an approximately 20% average error for natural frequencies and 45% average error over all static tests, necessitating further improvement of the model sophistication.

5 IDENTIFICATION AND PRIORITIZATION OF CONSTITUENTS

The structure of interest comprises two main constituents: the steel members and the connections. Though the material behavior of mild steel is widely studied, the bolted semirigid steel connections between beam and column are highly uncertain and are of great interest in the design and analysis communities. Lee and Moon (2002) and CEN (1997) provide provisions for approximate analysis of semirigid steel connections; however, many assumptions are made while establishing these provisions, such as small deformation in the connection, negligible deformation in the beam and column compared to the deformation in the connection, and negligible slip deformation.

Several investigators acknowledged and demonstrated that traditional assumptions of connections being either fixed or pinned can lead to significant errors in the analysis of static (Lee and Moon, 2002) and dynamic response (da Silva et al., 2008; Galvão et al., 2010; Tuürker et al., 2009; Wong et al., 1995), design and sizing of members (Lee and Moon, 2002), as well as design against progressive collapse (Liu et al., 2010). The findings obtained in Section 4.4 of this study also support these earlier studies that neither the fixed nor the pinned connections are acceptable to represent the two-bolt connection used in the steel frame studied herein. Therefore, while demonstrating the application of the proposed CPI metric, this study demonstrates mitigation of potential errors originating from the incomplete and inexact modeling of the semirigid steel connections through a rigorous modeling approach, where connections are parameterized (similar to the structural parameter identification for flexible connections presented in Wu and Li, 2006) and treated as constituents.

Similar to da Silva et al. (2008), three linear, rotational springs are added at each connection of the initial FE model (Model #1), which are used to capture rotations of the connection in all three directions. The springs are modeled using linear, COMBIN14 (spring-damper) elements (ANSYS, 2010). As the spring constants tend to zero, the connection behaves as a pin, and as the spring constants tend to infinite the connection becomes fixed. The stiffness of the bolted connections utilized in the frame structure, however, lie somewhere between these two extremes with unknown spring constants. Also, note that though this linear representation of semirigid springs supplies an improvement beyond a fixed or pinned connection, it fails to incorporate nonlinear effects.

The FE model can be further improved by developing three-dimensional, nonlinear FE models of the connections that account for friction between the members and pretension in the bolts (as it will be discussed in Section 6). These high-fidelity, nonlinear FE models of connections must be developed separately for the top, middle, and base connection; however, the limitations on project resources may inhibit model development of all three connections. Thus, to efficiently utilize the available resources, one must prioritize among these three possible constituent models to achieve the highest improvement in predictive capability. Such prioritization is achieved herein using the linear FE models of the constituent along with the CPI metric introduced in Section 3. The CPI requires a sensitivity analysis, and error estimate analysis, which are discussed in the following sections.

5.1 Sensitivity analysis

Herein, a global effect sensitivity analysis, ANOVA, is utilized. The selection of the plausible ranges, within which spring constants may vary, is critical in ANOVA; therefore, plausible ranges are determined by varying individual spring constants from free to an almost fixed condition one at a time, while the remaining spring constants are left constant at their nominal values. See, for instance, Figure 9, where the resulting natural frequencies are plotted as the strong axis bending stiffness constants for top level beams is varied. As one spring constant is varied, the natural frequencies vary between an upper bound (corresponding to a fixed connection) and a lower bound (corresponding to a pinned connection) in an asymptotic manner. Appropriate ranges for each spring constant can then be selected to ensure a semirigid behavior. As demonstrated in Figure 9, for the strong axis bending stiffness constant at the top level,

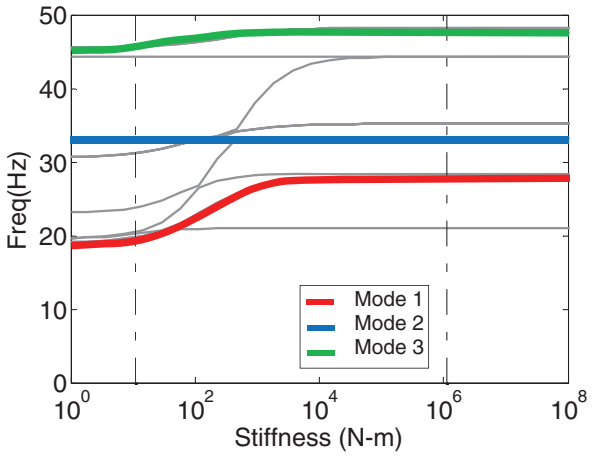

Fig. 9. Sensitivity of natural frequencies to strong axis bending stiffness constant at the top level.

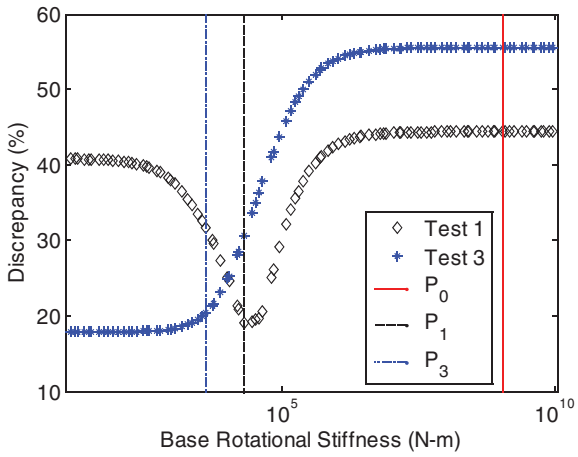

Fig. 10. Discrepancy versus Parameter 1 and selected parameter values for Static Tests 1 and 3.

the range is chosen to be 1.1×10^1–1.1×10^6 Nm as indicated with dashed lines.

After selecting the ranges for each stiffness constant, the sensitivities of natural frequencies and lateral displacements to the spring constants are analyzed through ANOVA. As seen in Figure 9, the analytically computed modes can swap their order when the stiffness constant is varied. For proper implementation of ANOVA on natural frequencies, a mode-pairing algorithm is developed, which operates on the spatial properties of each mode to properly reorder swapped modes according to a reference mode sequence. Table 5 lists the relative contribution of the stiffness constants to the overall variability in the predicted features, where the normalized sensitivities are summed for each connection level. Results indicate that the most sensitive constituents to model output are the middle, base, and top connections, respectively. The torsional stiffness constants are insensitive to the predicted features for all connection levels and thus, are not included in further discussion and are held at nominal (i.e., fixed) values.

5.2 Error analysis

The parameter of interest, P (see Table 5 for parameter numbers and corresponding constituents), is allowed to vary from 1.1×10^1 to 1.1×10^{10} Nm; α is chosen to be equal to 10%, γ is set to 0.5, n is 4, and β is chosen to be equal to 20%. One hundred scenarios are generated through Latin-Hypercube sampling. Figure 10 plots discrepancy as a function of spring constant for Parameter 1 for Static Tests 1 and 3, where the discrepancy is computed as a percentage of the experimental value for each experiment. The plot shows the initial parameter value and algorithm chosen parameter values for each experiment, respectively.

In Figure 10, P_0 represents the nominal value for the knob, which in this case is the stiffness constant of the base connection, and P_1 and P_3 represent the selected values, P_j, that minimize the discrepancy of Model #1 against Static Tests 1 and 3, respectively, according to Equations (4)–(7). P_1 shows a case where an absolute minimum discrepancy exists. Here, the

Table 5
Sensitivity analysis with normalized R^2 (%) values for each parameter

		Parameter number and description of stiffness	*Natural frequency*			*Max horizontal displacement*				*Total*
			Mode 1	*Mode 2*	*Mode 3*	Δ *Beam*^{Top}	Δ *Beam*^{Mid}	Δ *Column*	Σ	
Base	1	Rotational (strong axis)	47.7	36.9	65.3	18.1	7.3	37.2	212.3	212.3
	2	Torsional	0.00	0.00	0.00	0.00	0.00	0.00	0.01	
Middle	3	Rotational (strong axis)	33.2	51.8	23.1	17.1	5.9	35.2	166.3	251.6
	4	Rotational (weak axis)	2.2	0.02	0.17	0.08	82.8	0.00	85.3	
	5	Torsional	0.00	0.00	0.00	0.00	0.00	0.00	0.00	
Top	6	Rotational (strong axis)	12.0	11.1	11.2	13.4	4.0	27.6	79.2	136.1
	7	Rotational (weak axis)	4.9	0.30	0.32	51.3	0.02	0.00	56.9	
	8	Torsional	0.00	0.00	0.00	0.00	0.00	0.00	0.00	

Table 6
Error analysis of the three constituent models

Constituent	*Description of stiffness*	*EA(%)*	*Average constituent EA*
Base	Rotational (strong axis)	49.8	49.8
Middle	Rotational (strong axis)	51.2	59.1
	Rotational (weak axis)	66.9	
Top	Rotational (strong axis)	54.0	61.9
	Rotational (weak axis)	69.8	

Table 7
CPI for the three constituent models

Constituent	$\|SA\|$	$\|EA\|$	$\|UA\|$	*CPI*
Base connection	0.84	0.80	1.00	0.68
Middle connection	1.00	0.95	1.00	0.95
Top connection	0.54	1.00	1.00	0.54

selected parameter value, P_1, is the parameter value at the computed minimum discrepancy. P_3 shows a case where the discrepancy converges to a minimum. Here, the selected parameter value, P_3, is selected with a β value of 20%, that is, at the point where the discrepancy is 20% of the total possible reduction in discrepancy.

Table 6 lists the EA term computed as a percentage of the nominal value, P_0, according to Equations (2) and (3). For this application, the discrepancy tends to vary on a logarithmic scale for parameter values. Therefore, the percentages computed in Equation (3) are modified to represent log-based percentages. In Table 6, the EA terms are averaged for each connection. Results indicate that the largest error is associated with the top, middle, and base connections, respectively.

5.3 CPI calculation

The CPI values of the three connection models, calculated according to Equation (1), are listed in Table 7. As the knowledge level for each connection stiffness is low (i.e., constituents are highly uncertain), the UA terms for each connection are set to one. The SA and EA terms are normalized such that the highest value in each respective category is one. This normalization bounds all three terms in the CPI calculation between zero and one.

Table 7 prioritizes the three constituents in the following order of importance: middle, base, and top suggesting that the available resources should be devoted to obtain an improved representation of the middle connection first and the base connection next. Accordingly, three FE models with gradually improved representation of connections are developed in three successive phases: first, the initial frame FE model (Model #1) is coupled with only the middle connection model resulting in Model #2. Second, the base connection model is added to Model #2 to obtain Model #3. Finally, Model #4 is constructed by adding the top connection model to Model #3.

Fig. 11. FE connection models: top connection (left), middle connection (middle), and base connection (right).

6 DEVELOPMENT, VERIFICATION, AND VALIDATION OF CONSTITUENTS

6.1 Constituent model development

The connection models are developed as three-dimensional nonlinear FE models in ANSYS v.13.0. As suggested by Kim et al. (2007), Bursi and Jaspart (1997a, b, 1998), and Selamet and Garlock (2010), both the members of the connections and the bolts are modeled using three-dimensional solid finite elements (as opposed to simplified bolt models such as the coupled bolt model, spider bolt model, and no-bolt models as discussed in Kim et al. (2007)). SOLID187, a 10-noded tetrahedral element with quadratic displacement interpolation is used to model steel members and bolts. Effects of friction, represented using contact and target elements available in ANSYS v.13.0, CONTA174, and TARGET170, are modeled at all interfaces including: beam to column, bolt to column/beam, and bolt hole to bolt shank. The coefficient of friction is assumed for a Class A surface and set to 0.35 (AISC, 2008). The mesh size for all elements is selected through a mesh refinement study to assure that the numerical discretization is sufficiently fine to properly capture the deformation and stress concentration in critical regions. Figure 11 presents the FE models for all three connections.

As suggested by Citipitioglu et al. (2002), Kim et al. (2007), and Pirmoz et al. (2008, 2010), pretensioning of the bolts is included in the model. However, as opposed to using temperature or initial displacement methods commonly found in the literature, pretension elements available in ANSYS v.13.0, PRETS179, that directly apply a pretensioning force to the bolt volumes are implemented. This pretensioning force is determined by converting the torque applied on the bolts using

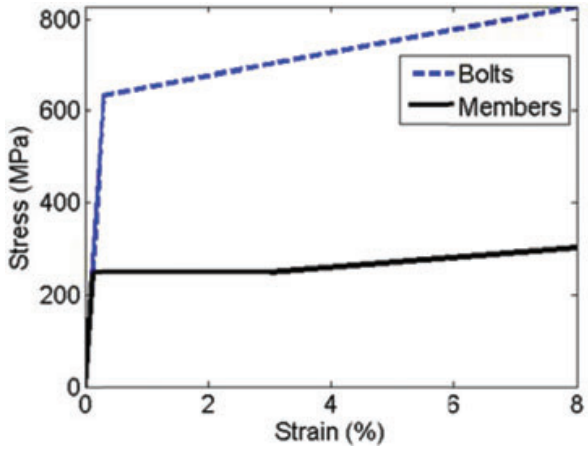

Fig. 12. Material models for bolts and steel frame members.

Equation (8) (Fastenal, 2005).

$$F_{PT} = \frac{T}{Kd} \tag{8}$$

where F_{PT} is the pretensioning force, T is the applied torque, K is the dimensionless nut factor, and d is the nominal bolt diameter. The recommended K for zinc-plated fasteners is 0.17–0.22 (Fastenal, 2005).

The beam and column material model is defined as a multilinear isotropic hardening model using the von Mises yield criterion and the typical stress–strain relationship shown in Figure 12 (Hibbeler, 2008). The bolts are modeled similarly except a bilinear model is utilized (Fastenal, 2005) (Figure 12).

6.2 Constituent model test-analysis correlations

To ensure that the constituent FE models exhibit sufficient fidelity, the model predictions are checked against experimental measurements. As the nonlinear features of the contact elements and pretensioning effects are not considered in modal analysis of the FE models (ANSYS only considers initial contact state), the clamping effects of the pretensioning are modeled by gluing a conical section formed through the beam and column between the bolt heads and nuts as described in Kim et al. (2007). Modal analysis is also conducted with scaled laboratory models of the connections supported with fixed boundaries (Figure 13), results of which are summarized in Figures 14 and 15 and Table 8.

The errors between the constituent FE model predictions and the experimental measurements of the first three natural frequencies range from a 10.9% average error for the middle connection to an average error of less than 7.8% for the top connection (Table 8). To validate the accuracy of the mode shapes predicted by the

Fig. 13. Connection test specimens: top connection (left), middle connection (middle), and base connection (right).

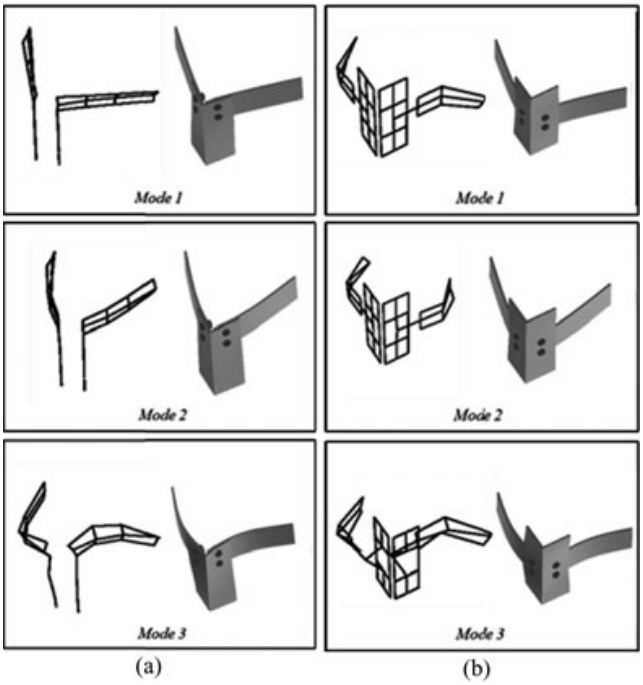

Fig. 14. Mode shapes (experimental on left, FE on right): top connection (a), middle connection (b).

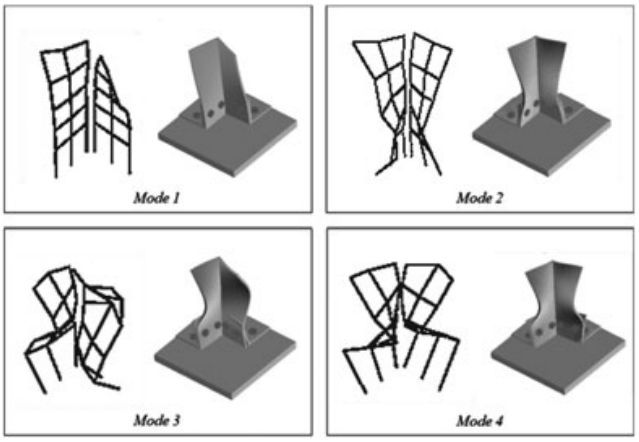

Fig. 15. Mode shapes (experimental on left, FE on right): base connection.

Table 8
Connection test-analysis correlation for connection models

	Mode	*$Freq_{exp}$ (Hz)*	*$Freq_{sim}$ (Hz)*	*% Error*
Base	1	473.4	425.6	10.1
	2	2043.6	2003.0	2.0
	3	2636.1	2295.4	12.9
	4	3005.4	2744.7	8.7
Middle	1	142.9	126.6	11.4
	2	157.0	135.1	13.9
	3	685.6	635.6	7.3
Top	1	79.7	75.1	5.8
	2	143.3	124.68	13.0
	3	459.0	438.4	4.5

Table 9
MAC analysis for base connection

		FE Model			
Experiment	*Mode*	*1*	*2*	*3*	*4*
	1	0.576	0.000	0.008	0.000
	2	0.008	0.783	0.010	0.019
	3	0.017	0.037	0.576	0.000
	4	0.000	0.054	0.000	0.764

Table 10
MAC analysis for middle connection

		FE Model		
Experiment	*Mode*	*1*	*2*	*3*
	1	0.870	0.004	0.030
	2	0.000	0.662	0.011
	3	0.005	0.000	0.880

Table 11
MAC analysis for top connection

		FE Model		
Experiment	*Mode*	*1*	*2*	*3*
	1	0.985	0.000	0.007
	2	0.045	0.908	0.002
	3	0.029	0.004	0.750

FE model, the MAC (used in Section 4.3 to check the orthogonality of the experimental modes) is calculated for each connection. In this case, the experimental mode shape vectors are calculated against the FE-predicted mode shape vectors. The results shown in Tables 9–11 demonstrate that with an average diagonal term value of 0.67, 0.80, and 0.88 for the base, middle, and top connection modes, respectively, the FE model-predicted

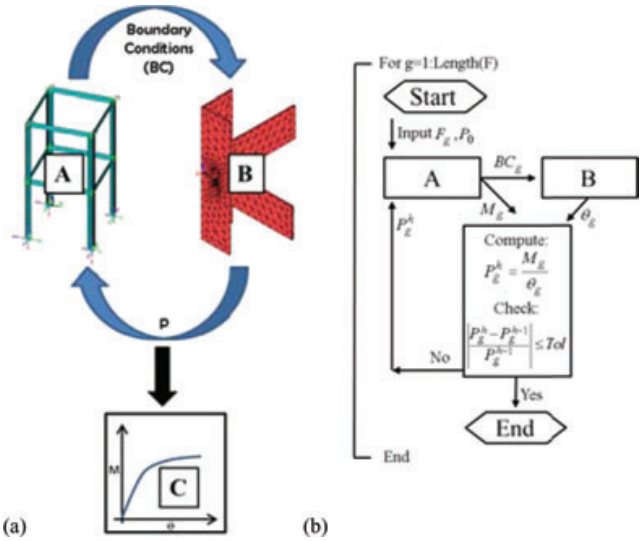

Fig. 16. Coupled process: (a) schematic representation and (b) numerical algorithm.

mode shape vectors are highly correlated to the experimental mode shape vectors and are an accurate representation of the experimentally collected modes. The accuracy shown in the dynamic testing provides sufficient evidence for the proper modeling of mass and stiffness distribution of the connections. Therefore, with an average error of less than 9% for the natural frequencies and an average diagonal MAC value of 0.77 across all modes of all models, the connection models are determined to be useful for making improved estimates of connection stiffness.

7 COUPLING OF CONSTITUENT MODELS

The coupling of the constituent connection models with the frame model is completed in two phases: the first step is an initial investment in computing the moment-rotation curves of the connections, and second step is coupling the trained moment-rotation curves with the frame model. The goal of the first phase is to determine the appropriate stiffness of the connections over a range of possible loading conditions; thus, in this phase, the deformations of columns in the frame must be taken into account. Determining the connection stiffness solely from the connection FE model with assumed boundary conditions would be invalid (note that this approach in literature, would be considered as weak [or loose] coupling). Therefore, a strong (or tight) coupling approach is taken and implemented using a Block Gauss-Siedel algorithm (Figure 2).

As shown in Figure 16, the moment-rotation curves are developed by first inducing a global loading

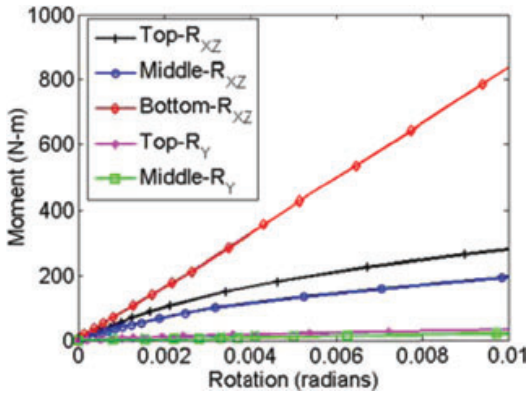

Fig. 17. Moment-rotation curves.

condition on the frame FE model at the midpoint of the beam for top and middle constituents and 1/8 point from the bottom of the column for the base constituent. The force, F_g, is a point load applied in the direction that critically affects the stiffness of each specific connection in the rotational direction of interest. The rotational stiffness constants are held at nominal (i.e., fixed) values, P_0. Next, displacements and rotations at the points where the connection models are cut off, BC_g, and the moment at the connection, M_g, are calculated by the frame FE model and passed to the coupling interface. The displacements and rotations at the cut-off points of the beams and columns are entered as inputs for the connection FE model, which in turn is executed to calculate the corresponding rotation at the connection, θ_g. Similar to approaches by Bursi and Jaspart (1997a, b) and Pirmoz et al. (2008), the rotation of the connection is computed by taking the relative difference between the rotation of the column and the rotation of the beam as expressed in Equation (9).

$$\theta_g = |\theta_{beam} - \theta_{column}| \tag{9}$$

The calculated rotation is then passed to the interface. The stiffness constant, P_g^h, at iteration h for load F_g is computed from the ratio of the computed moment to rotation, and then compared to the stiffness constant computed in the previous iteration, $h - 1$. The algorithm is terminated if the change in the computed stiffness constant between the last two iterations is less than a set threshold value (set to be 0.005 herein). Otherwise, the new stiffness constant is passed back to the frame model and the process is iterated until convergence is achieved.

The above-described process is repeated for increasing loads, F_g, to develop the moment-rotation curves, which are shown in Figure 17 for all rotational springs of interest. Note that for rotations less than 0.00017 radians, the moment/rotation data points for both the Top and Middle connection vertical bending (Top-R_{XZ} and Middle-R_{XZ}) are inconsistent with the linear portion of the respective moment-rotation curves, potentially due to the numerical round-off errors. Thus, these data points are removed from the curves for the analysis that follows.

In the second phase of the coupling process, the moment-rotation curves are directly incorporated into the frame FE model as nonlinear moment–rotation relationships using the nonlinear spring elements COMBIN39 available in ANSYS v.13.0.

The coupled solution is obtained for three variants of the frame FE model with increasing sophistication (Model #2–Model #4). The predictions of these models along with the initial FE model (Model #1) are compared against the static and modal experimental data as discussed in the next section.

8 RESULTS AND VALIDATION

All four variants of FE models are compared directly with modal and static experimental data. The disagreement between model predictions and experiments (referred to herein as discrepancy) is determined for each test as a percentage of the experimental measurements (Tables 12 and 13). Figure 18 compares the force–displacement plots of Static Test 1 for Model #4 and Model #1 to experimental data.

The computed discrepancy for each of the four models is compared for modal and static tests as shown in Tables 12 and 13. As the physics sophistication of the model increases from Model #1 to Model #4, the discrepancy between model predictions and experimental results decreases for nearly all predicted features, with the exception of Mode 2, which is underestimated by Model #4 approximately the same amount it is overestimated by Model #1.

Similarly, for the static case, the discrepancy between model predictions and experiments in general decreases as the model sophistication is increased. For instance, the discrepancy is significantly reduced by approximately 75% as the model sophistication is increased from Model #1 to Model #4 for Test 1. On average over all six static tests, Model #4 yields an agreement with a 29.59% discrepancy.

Recall that in Section 5.3, the three connection models are ranked using the CPI metric to determine the order to prioritize development of the connection FE models. In Tables 12 and 13, the gain in predictive accuracy on average is 6.41% from Model #1 to Model #2, 5.11% from Model #2 to Model #3, and 3.74% from Model #3 to Model #4 (Figure 19). These results indicating that the most information is gained by adding the middle connection model, then the bottom connection,

Table 12
Comparison of natural frequencies (Model #1–Model #4)

Mode	*Exp. (Hz)*	*Model #1 (Hz)*	*Disc. (%)*	*Model #2 (Hz)*	*Disc. (%)*	*Model #3 (Hz)*	*Disc. (%)*	*Model #4 (Hz)*	*Disc. (%)*
1	23.09	27.97	21.13	26.50	14.78	26.26	13.73	25.30	9.56
2	29.58	33.21	12.27	28.55	3.48	28.38	4.06	27.11	8.35
3	37.04	47.56	28.40	42.70	15.29	41.65	12.45	38.47	3.86

Note: Disc., discrepancy.

Table 13
Comparison of static displacements (Model #1–Model #4)

Test	*Model #1: mean disc. (%)*	*Model #2: mean disc. (%)*	*Model #3: mean disc. (%)*	*Model #4: mean disc. (%)*
1	44.42	33.12	18.91	11.08
2	84.83	89.00	79.68	73.73
3	55.60	52.57	48.74	46.29
4	46.75	37.35	25.37	18.05
5	24.26	19.39	17.42	16.43
6	18.93	13.98	12.75	11.96

Note: Disc., discrepancy.

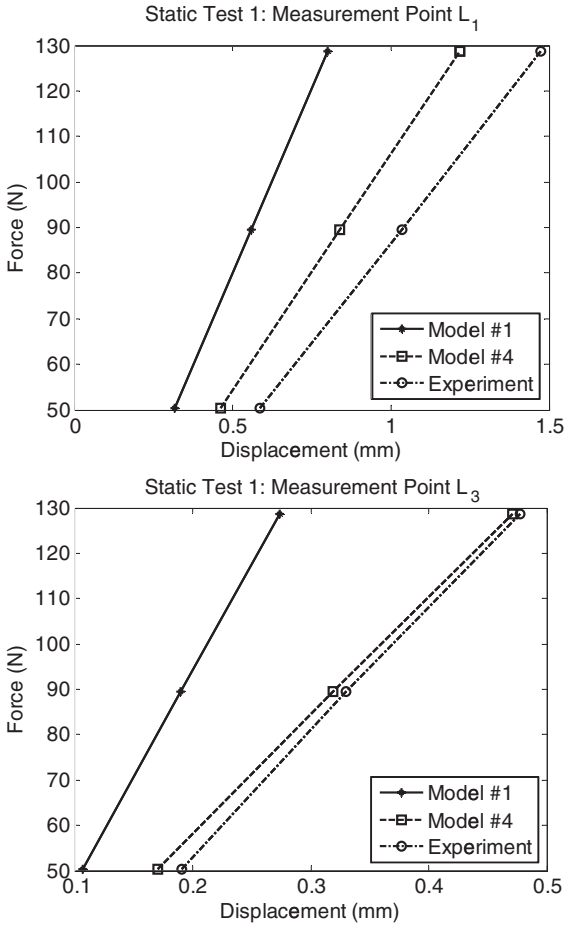

Fig. 18. Static test comparison: Model #1 versus #4.

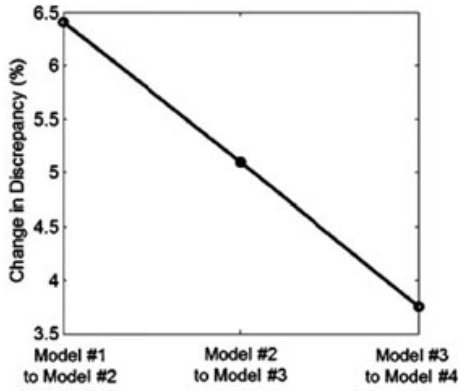

Fig. 19. Relative change in discrepancy with respect to physics sophistication.

Table 14
Comparison of discrepancy reduction for varying model increment cases

	Average reduction in mean discrepancy (%)		
Case constituent order	*Model #1 to Model #2*	*Model #2 to Model #3*	*Model #3 to Model #4*
M-B-T	6.41	5.11	3.74
M-T-B	6.41	3.08	5.77
B-M-T	3.47	8.04	3.74
B-T-M	3.47	3.27	8.51
T-M-B	3.05	6.44	5.77
T-B-M	3.05	3.70	8.51

and finally the top connection, are consistent with the code prioritization findings from CPI in Section 5.3.

To further validate the effectiveness of the CPI, all possible sequences of model development are investigated. Table 14 shows the average reduction in discrepancy for each incremental model development over all possible cases for the order, in which constituents (B—bottom connection, M—middle connection, and T—top connection) are improved through the coupling of a nonlinear FE connection model. The CPI selected path (highlighted in Table 14) is the only path that yields a monotonic increase in model accuracy; and thus, this path most efficiently improves the FE model. Therefore, in this application, the model accuracy is shown to be

improved as physics sophistication is increased, and the prioritization effort (CPI) is demonstrated to be effective in prioritizing constituents of a coupled model.

9 CONCLUDING REMARKS

Complex physical phenomena are amenable to decomposition in various forms depending upon the specific analysis or design objectives. Such decomposition into constituents can be steered by considerations regarding the physical, functional, or computational nature of the problem. Although we acknowledge the inherent inaccuracy of the numerical models used for simulations of complex coupled systems, the biases and uncertainties in model predictions can be reduced through further improvement of the simulation models, and rigorous verification, validation, and uncertainty quantification activities. There exists a need to prioritize these improvements such that resources are allocated to the model constituents that most effectively reduce model biases and uncertainties.

In this article, an index for code prioritization efforts of such complex numerical models, CPI, is developed for coupled numerical systems based upon fundamentals guiding the well-established PIRT ranking procedure. The CPI goes beyond the qualitative ranking system instituted in PIRT and supplies a quantitative assessment of the knowledge (uncertainty) and importance level (sensitivity) of a constituent phenomenon. Moreover, CPI incorporates an error analysis term (initial error). Through the combination and normalization of the three ranking categories (uncertainty, sensitivity, and initial error), the CPI represents a quantitative and defendable metric for ranking code prioritization efforts such that the largest reduction in model error can be achieved using minimal resources. The fundamental concept presented herein and its associated metrics requires an ability to parameterize the constituent models. Therefore, the study presented herein is most amenable for partitioned analysis procedures.

The CPI metric is demonstrated on a two-story steel frame with semirigid bolted connections. Predictions from an initial FE model (Model #1) of the steel frame indicate a high disagreement with experimental results. Deficiencies in the model are identified in the fixed beam-to-column connection assumptions. The stiffness of the three possible connection configurations (top, middle, and bottom) are treated as model constituents, and through the use of linear rotational springs implemented in the numerical model, these constituents are prioritized using the CPI metric. Next, high-fidelity, three-dimensional, nonlinear FE models of the connections are built for coupling with Model #1 in the order of their ranking as identified by CPI. Ultimately, through this coupling, Model #2 through Model #4 are obtained.

A comparison of modal and static test data to model predictions shows that as the physics of the model improve (from Model #1 to Model #4) the discrepancy reduces for nearly all test cases. Furthermore, the relative improvement from one sophistication to the next decreases as the model progresses from Model #1 to Model #4, indicting that the prioritization effort properly identified the order in which the constituent models should be improved.

Although the authors show the importance and usefulness of the proposed CPI metric, further work in the implementation and quantification of the uncertainty term is being considered. Additionally, the CPI metric proposed in this article is just one of many metrics that can be developed to incorporate all three terms, and investigations into the format, possible interactions among terms, and additional case studies is necessary. Also, as each component in CPI represents a specific facet of the model that may be more or less important to a specific project or research endeavor, user-defined weighting terms can be considered for each of the three components, respectively. However, future research is necessary to develop guidelines regarding the possible values (or ranges of values) for such weighting factors.

Additionally, while the connections used in the case study herein are not typical of traditional, large steel structures, they serve to demonstrate the validity of the CPI metric. Although the experimental campaign in the proof-of-concept application in this study is demonstrated in the linear/elastic regime, the proposed metric makes no assumptions that limit its application to such a regime. The proposed metric is versatile and generally applicable for any system with stable, nonchaotic responses (linear, nonlinear, elastic, inelastic, etc.).

ACKNOWLEDGMENTS

This work is funded by the United State Department of Energy: Nuclear Energy University Programs (Project: Predictive Maturity of Multiscale Simulation Models for Fuel Performance; Contract Number 00101999). The authors would like to thank the editor and the eight anonymous reviewers for their constructive comments and valuable suggestions to improve the quality of the article.

REFERENCES

Adeli, H. & Kamal, O. (1993), *Parallel Processing in Structural Engineering*, Elsevier Applied Science, London.

Advanced Reactor Research Infrastructure Assessment (ARRIA). (2003), Rev. 3, United States Regulatory Commission, Office of Nuclear Regulatory Research, 122–23.

Allemang, R. J. (2003), The modal assurance criterion (MAC): twenty years of use and abuse, *S V Sound and Vibration*, **37**(8), 14–23.

American Institute of Steel Construction (AISC). (2008), *Steel Construction Manual*, 13th edn, AISC, Chicago, 16, pp. 1–349.

ANSYS Mechanical APDL Element Reference (2010), Release 13.0., ANSYS, Inc., Canonsburg, PA, pp. 179–84, 1069–84.

Atamturktur, S., Hemez, F., Williams, B., Tome, C. & Unal, C. (2011), A forecasting metric for predictive modeling, *Computers and Structures*, **89**(23–24), 2377–87.

Avramova, M. N. & Ivanov, K. N. (2010), Verification, validation, and uncertainty quantification in multi-physics modeling for nuclear reactor design and safety analysis, *Progress in Nuclear Energy*, **52**, 601–14.

Bayarri, M. J., Berger, J. O., Paulo, R., Sacks, J., Cafeo, J. A., Cavendish, J., Lin, C. H. & Tu, J. (2007), A framework for validation of computer models, *Technometrics*, **49**(2), 138–54.

Boyack, B., Duffey, R., Griffith, P., Lellouche, G., Levy, S., Rohatgi, U., Wilson, G., Wulff, W., Zuber, N., Katsma, K. R., Hall, D. G., Shaw, R. A., Fletcher, C. D. & Boodry, K. S. (1989), *Quantifying Reactor Safety Margins: Application of Code Scaling, Applicability, and Uncertainty Methodology to a Large-Break, Loss-of-Coolant Accident*. US NRC Report, NUREG/CR-5249, Prepared by Idaho National Engineering Laboratory and managed by the U.S. Department of Energy, EG&G Idaho, Inc. Idaho Falls, ID.

Boyack, B.E. (2009), PIRT Workshop, Los Alamos National Laboratory presentation.

Bursi, O. S. & Jaspart J. P. (1997a), Benchmarks for finite element modeling of bolted steel connection, *Journal of Constructional Steel Research*, **43**(1–3), 17–42.

Bursi, O. S. & Jaspart J. P. (1997b), Calibration of a finite element model for isolated bolted end-plate steel connections, *Journal of Constructional Steel Research*, **44**(3), 225–62.

Bursi, O. S. & Jaspart J. P. (1998), Basic issues in the finite element simulation of extended end plate connections, *Computers and Structures*, **69**, 361–82.

Caracoglia, L., Noè, S. & Sepe, V. (2009), Nonlinear computer model for the simulation of lock-in vibration on long-span bridges, *Computer-Aided Civil and Infrastructure Engineering*, **24**, 130–44. ,

CEN, (1997), Eurocode 3 ENV-19931-1. Revised Annex J. *Design of Steel Structures*, Doc. CEN/TC250/SC3-N419E. European Committee for Standardization, Brussels, Belgium.

Citipitioglu, A. M., Haj-Ali, R. M. & White D. W. (2002), Refined 3D finite element modeling of partially-restrained connections including slip, *Journal of Constructional Steel Research*, **58**, 995–1013.

Cukier, R. L., Levine, H. B. & Schuler, K. E. (1978), Nonlinear sensitivity analysis of multiparameter model systems, *Journal of Computational Physics*, **26**, 1–42.

da Silva, J. G. S., de Lima, L. R. O., da Vellasco, P. C. G., de Andrade, S. A. L. & de Castro, R. A. (2008), Nonlinear dynamic analysis of steel portal frames with semi-rigid connections, *Engineering Structures*, **30**, 2566–79.

Diamond, D. J. (2006), Experience using Phenomena Identification and Ranking Technique (PIRT) for nuclear analysis, Brookhaven National Laboratory Report, BNL-76750–2006-CP, Upton, NY.

Eurocode 3 ENV-1993–1-1. (1993), European Committee for Standardisation. Revised Annex J. Design of Steel Structures. Doc. CEN/TC250/SC3-N419E.

Farajpour, I. & Atamturktur, S. (2012), Optimization-based strong coupling procedure for partitioned analysis, *ASCE Journal of Computing in Civil Engineering*, **26**(5), 648–60.

Fastenal (2005), Technical Reference Guide, s7028, rev. 9. Available at: http://www.fastenal.com/content/documents/FastenalTechnicalReferenceGuide.pdf, accessed May 14, 2012.

Felippa, C. A., Park, K. C. & Farhat, C. (2001), Partitioned analysis of coupled mechanical systems, *Computer Methods in Applied Mechanics and Engineering*, **190**, 3247–70.

Fernandez, M. A. & Moubachir, M. (2005), A Newton method using exact Jacobians for solving fluid–structure coupling, *Computers and Structures*, **83**, 127–42.

Frey, H. C. & Patil, S. R. (2002), Identification and review of sensitivity analysis methods, *Risk Analysis*, **22**(3), 553–78.

Galvão, A. S., Silva, A. R. D., Silveira, R. A. M. & Gonçalves, P. B. (2010), Nonlinear dynamic behavior and instability of slender frames with semi-rigid connections, *International Journal of Mechanical Sciences*, **52**, 1547–62.

Heil, M. (2004), An efficient solver for the fully coupled solution of large-displacement fluid–structure interaction problems, *Computer Methods in Applied Mechanics and Engineering*, **193**, 1–23.

Hemez, F. M., Atamturktur, S. H. & Unal, C. (2010), Defining predictive maturity for validated numerical simulations, *Computers and Structures*, **88**, 497–505.

Hibbeler, R. C. (2008), *Mechanics of Materials*, 7th edn, Pearson Prentice Hall, Upper Saddle River, NJ, 90,pp.

Higdon, D., Gattiker, J., Williams, B. & Rightley, M. (2008), Computer model calibration using high-dimensional output, *Journal of the American Statistical Association*, **103**(482), 570–83.

Ibrahimbegović, A., Knopf-Lenoir, C., Kučerová, A. & Villon, P. (2004), Optimal design and optimal control of elastic structures undergoing finite rotations and deformations, *International Journal for Numerical Methods in Engineering*, **61**, 2428–60.

Jiang, X. & Mahadevan, S. (2007), Bayesian risk-based decision method for model validation under uncertainty, *Reliability Engineering and System Safety*, **92**, 707–18.

Joosten, M. M., Dettmer, W. G. & Peric, D. (2009), Analysis of the Block Gauss–Seidel solution procedure for a strongly coupled model problem with reference to fluid–structure interaction, *International Journal for Numerical Methods in Engineering*, **78**, 757–78.

Jung, B. (2011), A hierarchical framework for statistical model validation of engineered systems. Dissertation, University of Maryland.

Kassiotis, C., Ibrahimbegović, A., Niekamp, R. & Matthies, H. (2011), Partitioned solution to nonlinear fluid-structure interaction problems. Part I: Implicit coupling algorithms and stability proof, *Computational Mechanics*, **47**, 305–23.

Kim, J., Yoon, J.-C. & Kang, B.-S. (2007), Finite element analysis and modeling of structure with bolted joints, *Applied Mathematical Modelling*, **31**, 895–911.

Korel, B. (2009), Experimental comparison of code-based and model-based test prioritization, *IEEE International Conference on Software Testing Verification and Validation Workshops*, Denver, CO, April 1–4, 77–84.

Kutay, M. E. & Aydilek, A. H. (2009), Pore pressure and viscous shear stress distribution due to water flow within

asphalt pore structure, *Computer-Aided Civil and Infrastructure Engineering*, **24**, 212–24.
Larson, J., Jacob, R. & Ong, E. (2005), The model coupling toolkit: a new Fortran90 toolkit for building multi-physics parallel coupled models, *International Journal of High Performance Computer Applications*, **19**(3), 277–92.
Larson, J. W. (2009), Ten organising principles for coupling in multiphysics and multiscale models. *ANZIAM Journal*, **48**, C1090–C1111.
Lee, S. S. & Moon, T.-S. (2002), Moment-rotation model of semi-rigid connections with angles, *Engineering Structures*, **24**, 227–37.
Leiva, J. S., Blanco, P. J. & Buscaglia, G. C. (2010), Iterative strong coupling of dimensionally heterogeneous models, *International Journal for Numerical Methods in Engineering*, **81**, 1558–80.
Liu, Y., Xu, L. & Grierson, D. E. (2010), Influence of semi-rigid connections and local joint damage on progressive collapse of steel frameworks, *Computer-Aided Civil and Infrastructure Engineering*, **25**, 184–204.
Macdonald, J. H. G. (2009), Lateral excitation of bridges by balancing pedestrians, in *Proceedings of the Royal Society A – Mathematical Physical and Engineering Sciences*, **465**, 1055–73.
Mahjoubi, N., Gravouil, A. & Combescure, A. (2009), Coupling subdomains with heterogeneous time integrators and incompatible time steps, *Computational Mechanics*, **44**, 825–43.
Mahjoubi, N., Gravouil, A., Combescure, A. & Greffet, N. (2011), A monolithic energy conserving method to couple heterogeneous time integrators with incompatible time steps in structural dynamics, *Computer Methods in Applied Mechanics and Engineering*, **200**, 1069–86.
Matthies, H. G., Niekamp, R. & Steindorf, J. (2006), Algorithms for strong coupling procedures, *Computer Methods in Applied Mechanics and Engineering*, **195**, 2028–49.
Matthies, H. G. & Steindorf, J. (2002a), Fully coupled fluid–structure interaction using weak coupling, *Proceedings in Applied Mathematics and Mechanics*, **1**(1), 37–38.
Matthies, H. G. & Steindorf, J. (2002b), Partitioned but strongly coupled iteration schemes for nonlinear fluid–structure interaction, *Computers and Structures*, **80**, 1991–99.
Matthies, H. G. & Steindorf, J. (2003), Partitioned strong coupling algorithms for fluid–structure interaction, *Computers and Structures*, **81**, 805–12.
Moaveni, B., Conte, J. P. & Hemez, F. M. (2009), Uncertainty and sensitivity analysis of damage identification results obtained using finite element model updating, *Computer-Aided Civil and Infrastructure Engineering*, **24**(5), 320–34.
Oberkampf, W. L. & Barone, M. F. (2006), Measures of agreement between computation and experiment: validation metrics, *Journal of Computational Physics*, **217**, 5–36.
Olivier, T. J. & Nowlen, S. P. (2008), A Phenomena Identification and Ranking Table (PIRT) exercise for nuclear power plant fire modeling applications, US NRC Publication and Sandia National Laboratories Report, NUREG/CR-6978, SAND2008–3997P, Sandia National Laboratories, Albuquerque, NM, 1–31.
Park, K. & Felippa, C. A. (1983), Partitioned analysis of coupled systems, *Computational Methods for Transient Analysis*, **1**, 157–219.
Pirmoz, A., Ahmadi, M. M., Valadi, E., Farajkhah, V. & Balanoji, S. R. (2010), Performance of the PR connections under combined axial-tension and moment loading, *Electronic Journal of Structural Engineering*, **10**, 66–73.
Pirmoz, A., Daryan, A. S., Mazaheri, A. & Darbandi, H. E. (2008), Behavior of bolted angle connections subjected to combined shear force and moment, *Journal of Constructional Steel Research*, **64**, 436–46.
Provenzano, P. (2003), A fuzzy-neural network method for modeling uncertainties in soil-structure interaction problems, *Computer-Aided Civil and Infrastructure Engineering*, **18**, 391–411.
Qian, L. & Zhang, H. (1993), An improved non-reflecting boundary method for soil-structure interaction analysis, *Computer-Aided Civil and Infrastructure Engineering*, **8**(4), 291–97.
Ramanath, G. (2011), Collaborative research: understanding mechanical and thermal properties and their coupling at nanomolecularly modified metal-ceramic, NSF Award Abstract #1100933.
Rebba, R., Mahadevan, S. & Huang, S. (2006), Validation and error estimation of computational models, *Reliability Engineering & System Safety*, **91**, 1390–97.
Richardson, M. H. & Formenti, D. L. (1982), Parameter estimation from frequency response measurements using rational fraction polynomials, in *Proceedings of the 1st International Modal Analysis Conference*, Orlando, FL.
Rugonyi, S. & Bathe, K. J. (2001), On finite element analysis of fluid flows fully coupled with structural interactions, *Computer Modeling in Engineering and Sciences*, **2**, 195–212.
Selamet, S. & Garlock, M. (2010), Guidelines for modeling three dimensional structural connection models using finite element methods, *International Symposium: Steel Structures: Culture & Sustainability* 2010, Istanbul, Turkey, Paper No. 14.
Tregoning, R. T., Apps, J. A., Chen, W., Delegard, C. H., Litman, R. & MacDonald, D. D. (2009), Phenomena Identification and Ranking Table evaluation of chemical effects associated with generic safety issue 191, US NRC Publication, NUREG-1918, U.S. Nuclear Regulatory Commission, Washington DC, 1–97.
Tuürker, T., Kartal, M. E., Bayraktar, A. & Muvafik, M. (2009), Assessment of semi-rigid connections in steel structures by model testing, *Journal of Constructional Steel Research*, **65**, 1538–47.
Unal, C., Williams, B., Hemez, F., Atamturktur, S. H. & McClure, P. (2011), Improved best estimate plus uncertainty methodology, including advanced validation concepts, to license evolving nuclear reactors. *Nuclear Engineering and Design*, **241**, 1813–33.
Wang, D., Gao, S. Q., Kasperski, M., Liu, H. P. & Jin, L. (2011), Simulation of the dynamic characteristics of the coupled system structure, *Applied Mechanics and Materials*, **71–78**, 1507–10.
Wang, J. G., Nogami, T., Dasari, G. R. & Lin, P. Z. (2004), A weak coupling algorithm for seabed–wave interaction analysis, *Computer Methods in Applied Mechanics and Engineering*, **193**, 3935–56.
Williams, B. J., Loeppky, J. K., Moore, L. M. & Macklem, M. S. (2011), Batch sequential design to achieve predictive

maturity with calibrated computer models. *Reliability Engineering and System Safety*, **96**, 1208–19.

Wong, C. W., Mak, W. H. & Ko, J. M. (1995), System and parametric identification of flexible connections in steel framed structures, *Engineering Structures*, **17**(8), 581–95.

Wu, J. R. & Li, Q. S. (2006), Structural parameter identification and damage detection for a steel structure using a two-stage finite element model updating method, *Journal of Constructional Steel Research*, **62**, 231–39.

Xiong, T., Zhang, M., Shu, C. W., Wong, S. C. & Zhang, P. (2011), High order computational scheme for a dynamic continuum model for bi-directional pedestrian flows, *Computer-Aided Civil and Infrastructure Engineering*, **26**(4), 297–310.

Zapico, J. L., Gonzalez-Buegla, A., Gonzalez, M. P. & Alonso, R. (2008), Finite element model updating of a small steel frame using neural networks, *Smart Materials and Structures*, **17**(045016), 1–11.

Zeyao, M. & Lianxiang, F. (2004), Parallel flux sweep algorithm for neutron transport on unstructured grid, *The Journal of Supercomputing*, **30**, 5–17.

Zhang, Q. & Hisada, T. (2004), Studies of the strong coupling and weak coupling methods in FSI analysis, *International Journal for Numerical Methods in Engineering*, **60**, 2013–29.